Wideband Low Loss Bending-Resistance Hollow-Core Fiber With Hybrid Claddings of Antiresonance and Photonic Bandgap Guidance Mechanisms

Yundong Hao, Huiyi Guo, Yong You, Zhi Wang, and Yan-Ge Liu

***Abstract*—Hollow-core anti-resonant fibers (HC-ANF) have the advantages of low scattering loss, wide bandwidth and simplicity of preparation, but are sensitive to bend, which limits their practical applications. On the contrary, hollow-core photonic bandgap (HC-PBGF) fibers have lower confinement loss and more robust bending characteristic, but exhibit unavoidable high scattering loss, influence of surface modes and stricter manufacturing processes. In this article, a novel hollow-core hybrid cladding fiber (HC-HBCF) which consists of anti-resonant circular tubes of inner cladding and periodically arranged air holes of outer cladding is proposed and investigated numerically. The results show that combining the claddings of antiresonance and photonic bandgap guidance mechanisms can effectively reduce the mode confinement loss by five and six orders of magnitude compared to the fibers with two claddings alone respectively. The proposed HC-HBCF exhibits similar excellent low scattering loss and spectral flatness as the single-tube anti-resonant fiber. Specifically, the proposed HC-HBCF exhibits the confinement loss of 5×10^{-5} dB/km at 1550 nm and a total loss of 0.1 dB/km from 1430 nm to 1770 nm. Meanwhile, the hybrid cladding fiber has an outstanding bending property with a bending loss of 0.16 dB/km at a small bending radius of 2 cm. The mode properties of HC-HBCF are also calculated and analyzed, indicating that the hybrid cladding fiber has a unique potential in controlling modal content.**

***Index Terms*—Optics fibers, hollow-core fibers, photonic bandgap, antiresonance.**

I. Introduction

HOLLOW-CORE fibers have been widely investigated and fabricated in recent years due to their unique property of guiding light in the air core [1], which gives it many advantages over traditional solid-core fibers such as low nonlinearity, low latency, high threshold for material damage, ultralow Rayleigh scattering [2], [3], [4], [5], [6]. These characteristics greatly promote the application of hollow-core fibers in fields of data transmission [7], [8], high-power laser delivery [9], [10], OAM mode transmission [11], and gas-based nonlinear optics [12], [13], [14].

Generally, hollow core fibers are divided into two categories due to the difference of guidance mechanism. One is hollow-core photonic bandgap fiber, which confines light in air core via the photonic bandgap formed by a periodic structure of the cladding [15]. The main loss in HC-PBGF is surface scattering loss (SSL) caused by the surface roughness of frozen capillary [16]. The SSL can be reduced by increasing core radius or introducing anti-resonant wall thickness. However, enlarging core size will introduce more core modes [17], and increasing wall thickness will introduce more surface modes to couple with the core modes thus affecting available bandwidth [18]. The lowest loss of reported HC-PBGF is 1.7 dB/km with a total available bandwidth of 70 nm due to the existence of surface modes [19]. Meanwhile, studies show that surface modes can be removed from the bandgap as the thickness of silica ring surrounding core is half of that of the thin cladding struts. Based on this, a 19-cell HC-PBGF with low loss (3.5 dB/km) and broadband (160 nm) was fabricated and demonstrated in data transmission experiment [5]. Obviously, the unique properties of air-guiding modes and bending-resistance for HC-PBGF greatly promote its integrated applications for short distance such as fiber gyroscope. However, the loss of currently fabricated HC-PBGF still not reach ideal level due to the surface scattering loss, limiting its long-distance application such as data transmission. Therefore, the fabrication of HC-PBGF with large core, ultra-low loss and wide bandwidth without influence of surface modes is necessary for its application in data transmission, which will bring great challenges in mode control and manufacturing process.

On the other hand, hollow-core anti-resonant fiber confines light in air core by the combination of anti-resonance effect and inhibited-coupling effect [20], [21]. Kagome fiber [22] is the earliest hollow-core inhibited-coupling fiber. Subsequent simulations and experiments proved the loss independence on number of cladding layer and the crucial role of core shape in loss performance [23], [24], and then a single-ring tubular-lattice fiber was fabricated in the mid-infrared spectral region [25]. After that, it was found that the node-less and nested structure can further reduce the confinement loss [26]. A conjoined-tube HC-ANF was demonstrated the loss of 2 dB/km in 2018 [27] and a six nested tubes HC-ANF with loss of 0.28 dB/km was obtained

Manuscript received 5 September 2023; revised 3 October 2023; accepted 15 October 2023. Date of publication 19 October 2023; date of current version 27 October 2023. This work was supported by the National Natural Science Foundation of China under Grant 61835006. *(Corresponding author: Yan-Ge Liu.)*

The authors are with Tianjin Key Laboratory Micro-Scale Optical Information Science and Technology, Institute of Modern Optics, Nankai University, Tianjin 300350, China (e-mail: hydnku@163.com; nkughy@outlook.com; youyongmail@163.com; zhiwang@nankai.edu.cn; ygliu@nankai.edu.cn).

Digital Object Identifier 10.1109/JPHOT.2023.3325481

at 1550 nm in 2020 [28]. Recently, a double-nested anti-resonant hollow core fiber was fabricated and demonstrated a minimum reported loss of 0.174 dB/km [29]. Besides, HC-ANF with various cladding structures are designed and numerically investigated [30], [31], [32]. Compared to HC-PBGF, HC-ANF exhibits lower surface scattering loss, wider bandwidth unaffected by surface modes and better modal content, but more sensitive to bending, which limits their applications. Accordingly, designing and fabricating a high-performance hollow-core fiber with ultralow loss, wide bandwidth, low bending loss and outstanding modal content is urgently needed, and combination of photonic bandgap and anti-resonance guidance mechanisms is one of the potential under-studied approaches to address the problem. A hybrid-lattice hollow core fiber that consists of Kagome and tubular cladding lattices was proposed and fabricated in 2021 [33]. Despite of low loss and single-mode operation, the combination of two large periodic lattices sacrifices its bending properties. A novel hollow core fiber which combines an anti-resonant structure with a multilayer Bragg structure have been designed and numerically investigated in MIR (5.6 μm−10 μm) [34]. However, due to the Bragg structure and polymer materials used in outer layer, this design only realizes the combination of photonic bandgap and anti-resonance guidance mechanism in MIR. An effective combination of anti-resonant structure and photonic bandgap structure formed by periodically arranged air holes on silica in traditional HC-PBGF has never been reported or studied.

In this article, we propose a novel hollow core hybrid cladding fiber, which consists of the anti-resonant tubes and periodically arranged air holes. The two different claddings with antiresonance and photonic bandgap guidance mechanisms are effectively combined, greatly reducing the confinement loss that is five and six orders of magnitude lower than those of two fibers with separate cladding respectively. Moreover, the proposed fiber exhibits a wide bandwidth of 350 nm with a total loss of 0.1 dB/km, which indicates that the anti-resonant structure of inner cladding can make the core mode as little as possible to be affected by innermost structure of the bandgap cladding. An outstanding bending property is also proved in our HC-HBCF with a loss of 0.16 dB/km at 2 cm bending radius. Meanwhile, the proposed fiber presents a better modal content compared to the HC-PBGF with the same core radius. These results indicate that our proposed fiber is a promising candidate for obtaining high-performance hollow-core fiber with ultralow loss, wide bandwidth, low bending loss and outstanding modal content.

II. Fiber Design

The cross-section of proposed HC-HBCF is shown in Fig. 1. The cladding consists of anti-resonant structure of inner cladding and photonic bandgap structure of outer cladding, which effectively combines the guidance mechanisms of anti-resonance and photonic bandgap. The outer cladding is same as conventional HC-PBGF cladding, consisting of periodically arranged air holes on pure silica material. It is formed by removing eight layers of air holes from center to ensure that the fiber structure has a large core radius after adding the anti-resonant

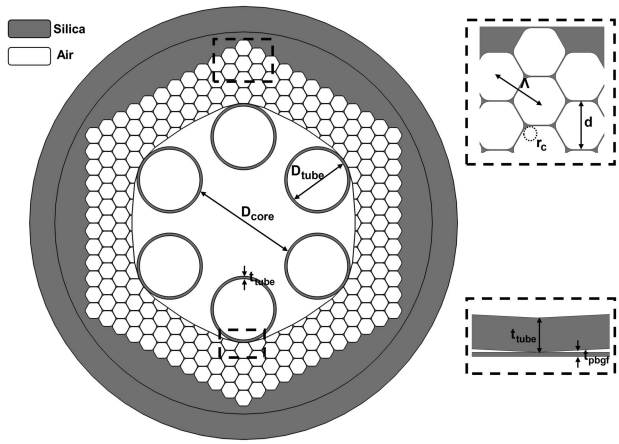

Fig. 1. Cross-section of proposed HC-HBCF with anti-resonant circular tubes and periodically arranged air holes.

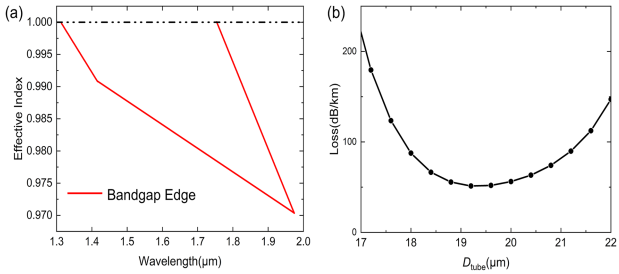

Fig. 2. (a) Photonic bandgap of outer cladding calculated using PWEM ($\Lambda = 5\ \mu$m, $d = 4.8\ \mu$m, $r_c = 1\ \mu$m). (b) Loss with respect to the tube dimeter D_{tube} in a single-ring anti-resonant fiber with a fixed outer diameter at 1550 nm.

structure, which is a crucial condition for HC-ANF to achieve low loss. As the outer cladding has C6v symmetry, we choose six anti-resonant tubes that also exhibits C6v symmetry as inner anti-resonant structure to maximally fit the bandgap cladding in terms of geometry and light guiding mechanism. We choose single-ring circular tubes instead of other nested structure to avoid guiding modes due to thick silica at contact position of inner and outer claddings. Once the six circular tubes are well realized in combination with photonic bandgap cladding, other anti-resonant structures will also be implemented in the same way.

The fiber parameters include core dimeter D_{core}, tube dimeter D_{tube}, tube thickness t_{tube}, which determine the bandwidth and performance of inner anti-resonant cladding, and lattice constant Λ, diameter of air holes d, hexagonal air hole circular angle radius r_c that determine the position and bandwidth of photonic bandgap. To achieve both guidance mechanisms simultaneously, the low-loss transmission band of inner and outer cladding must effectively overlap and it guides us in the selection of structural parameters. Specifically, we calculated the bandgap under different parameters of Λ, d, r_c using the plane wave expansion method (PWEM) and finally set them to 5 μm, 4.8 μm, 1 μm, respectively. The calculated photonic bandgap under these specific parameters is shown in Fig. 2(a) from which we can see that 1550 nm is in the middle of bandgap, and the width of bandgap is nearly 400 nm that absolutely meet application

needs in the near-infrared region. Meanwhile, t_{pbgf} is set to 50 nm, which is half of that of the thin cladding struts to avoid Fano resonance due to thick contact points with inner anti-resonant circular tubes.

On the other hand, the transmission band of inner cladding is determined by the thickness of circular tube, from which we can calculate the resonant wavelength, and the region of two adjacent resonant wavelengths is low-loss transmission band. The resonant wavelength can be calculated by [26]:

$$t = \frac{2\pi\lambda}{m}\sqrt{\left(n_g^2 - 1\right)} \tag{1}$$

Where t is thickness of tubes, n_{g} is refractive index of glass, λ is operating wavelength, m is an integer which indicates the order of transmission band. We choose m as 1 and t as 400 nm for lower loss and wider bandwidth around 1550 nm. Moreover, before anti-resonant structure is added, the large air area in center is formed by removing eight layers of air holes of the bandgap cladding. When the bandgap cladding structure is determined, the size of large air area in center is determined, which brings a geometrical relationship:

$$\frac{D_{\mathrm{core}}}{2} + 2 * t_{\mathrm{tube}} + D_{\mathrm{tube}} = 7\Lambda + \frac{d}{2} \tag{2}$$

Therefore, we can optimize inner cladding structure in a single-ring anti-resonant fiber with a fixed outer diameter to obtain the best performance of inner cladding and result is shown in Fig. 2(b). It is noticed that the anti-resonant fiber has minimum loss at 1550 nm when D_{tube} is 19.2 μm. Therefore, D_{tube} and D_{core} in our HC-HBCF are set to 19.2 μm, 35 μm respectively.

III. Result and Discussion

The numerical simulation in this work is carried out using COMSOL multi-physics which is based on the finite element method. The maximum mesh size of air and silica area is $\lambda/4\mathrm{n}$ and $\lambda/6\mathrm{n}$ respectively, and a perfectly-matched layer (PML) is set outside the fiber domain to obtain accurate imaginary part of mode eigenvalues. The confinement loss (CL) is calculated by following expression as [35]:

$$\mathrm{CL}[\mathrm{dB/km}] = \frac{40\pi \mathrm{Im}(n_{\mathrm{eff}})}{\ln(10)\lambda[\mathrm{m}]}10^3 \tag{3}$$

Where $\mathrm{Im}(n_{\mathrm{eff}})$ is imaginary part of mode effective refractive index. To ensure the accuracy of numerical calculations, we performed convergence tests for the maximum mesh size parameter n and the PML thickness. Fig. 3 shows the variation of confinement loss for the proposed fiber with n and PML thickness at 1550 nm. It can be seen that when n is greater than 0.5 and PML thickness is greater than 1 μm, the confinement loss of proposed fiber becomes stable, so we choose n = 1, PML = 10 μm in our study.

Moreover, the surface scattering loss (SSL) needs to be considered for hollow core fibers and is calculated using [26]:

$$\mathrm{SSL}[\mathrm{dB/km}] = \eta F\left(\frac{\lambda[\mu\mathrm{m}]}{\lambda_0}\right)^{-3} \tag{4}$$

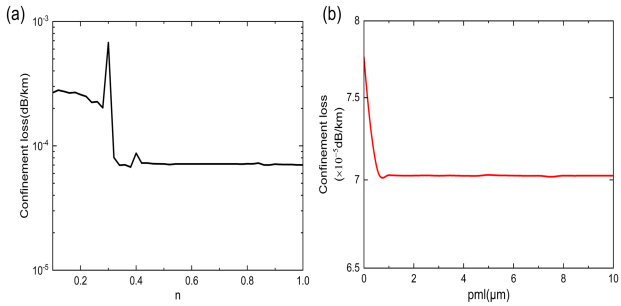

Fig. 3. Convergence test: confinement loss of our proposed HC-HBCF at 1550 nm for (a) the mesh size where the maximum mesh size in the silica and air regions are $\lambda/(6\mathrm{n})$ and $\lambda/(4\mathrm{n})$, respectively, and (b) the perfectly-matched layer thickness.

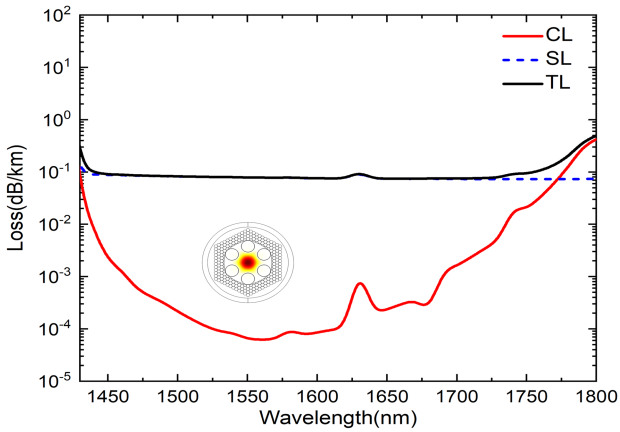

Fig. 4. Loss performance of proposed HC-HBCF, including confinement loss (CL), scattering loss (SL) and total loss (TL).

Where F quantifies the overlap of core mode with silica boundary, and $\eta = 300$ is a calibration factor when λ_0 is 1550 nm. However, due to existence of anti-resonant structure in HC-HBCF, the value of scattering loss calculated by above formula will be larger [28]. Here, we still use this formula for systematic research

Fig. 4 shows the calculated loss performance of proposed HC-HBCF. It is noticed that the proposed fiber can guide light with extremely low loss in the range of 1420 nm ~1800 nm, where the lowest total loss (TL) is 0.07 dB/km at 1550 nm, and exhibits a wide bandwidth of 350 nm with a total loss of 0.1 dB/km.

To further study and illustrate the characteristic of hybrid cladding fiber, we calculated and compared HC-ANF and HC-PBGF with the same cladding structure parameters. The single ring negative curvature fiber with six tubes (SR-NCF) shown in Fig. 5(b) is formed by simply removing the outer bandgap cladding of proposed HC-HBCF, and its core size, anti-resonant tube radius and tube thickness are the same as those of the HC-HBCF. The PBGF-a shown in Fig. 5(c) is formed by simply removing the inner cladding of proposed HC-HBCF, and its lattice period and air-filling fraction are the same as the bandgap cladding of HC-HBCF. The PBGF-b shown in Fig. 5(d) has the

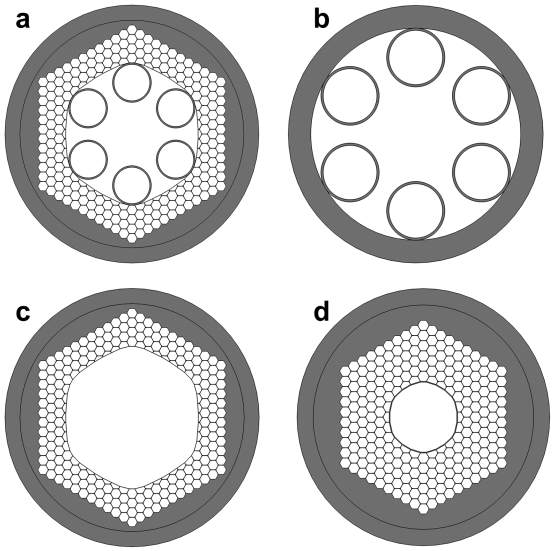

Fig. 5. Geometries considered in calculations. (a) Proposed HC-HBCF; (b) SR-NCF (a single ring negative curvature fiber with six tubes); (c) PBGF-a (a HC-PBGF with four layers of air holes); (d) PBGF-b (a HC-PBGF with the same core radius and wall thickness as proposed HC-HBCF).

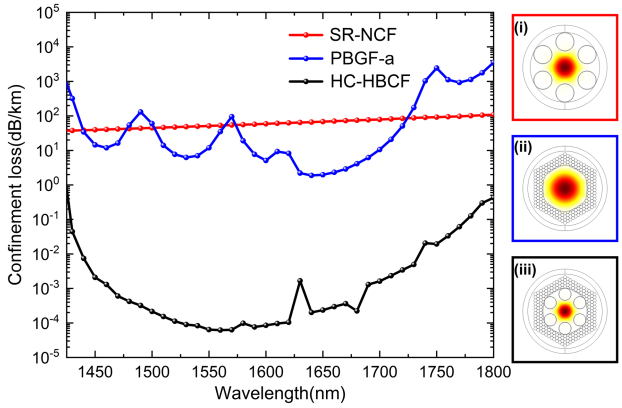

Fig. 6. Comparison of the confinement loss between HC-HBCF, SR-NCF and PBGF-a. The fundamental mode field profiles of three fibers are shown in the right-side panel.

same core size as HC-HBCF, and the core wall thickness is same as the anti-resonant tube thickness of HC-HBCF.

A. Loss Characteristics

Fig. 6 shows the confinement loss spectra of HC-HBCF and other two hollow-core fibers mentioned above. It is noted that the SR-NCF exhibits the highest CL among all those fibers due to simple cladding structure that there is only one layer of anti-resonant element which cannot effectively confine light within the fiber core. The CL of SR-NCF increases gradually from 30 dB/km (1430 nm) to 100 dB/km (1800 nm) with increase of wavelength, and the spectrum shows flat behavior over bandwidth. A single ring anti-resonant fiber with similar structural parameters was fabricated and used for data transmission [36], which exhibits same loss level as the simulated SR-NCF.

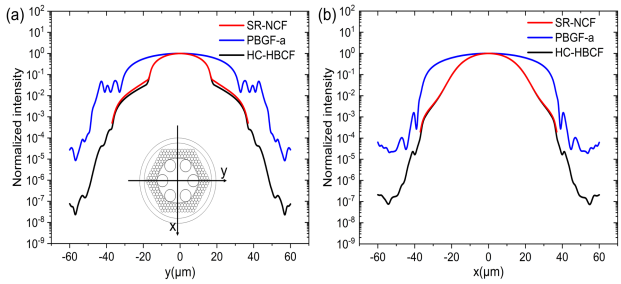

Fig. 7. (a) Variation of normalized intensity along the y axes for three fibers at fixed x of 0 μm. (b) Variation of normalized intensity along the x axes for three fibers at fixed y of 0 μm.

Meanwhile, it has been proved that the CL of photonic bandgap fiber is strictly related to the number of cladding air holes layers. Therefore, as blue curve shown in Fig. 6, the PBGF-a shows loss above 1 dB/km over entire bandgap as it only has 4-layer cladding air holes, which exhibits the same order of magnitude as the results calculated in [37]. Besides, due to the coupling between core mode and surface mode, the core mode has energy leakage at coupling wavelengths, leading to a great increasement of CL.

Surprisingly, when we only combine the cladding of above two fibers through direct contact, the HC-HBCF exhibits an amazing improvement in confinement loss. It presents a CL of 6×10^{-5} dB/km at 1550 nm, which is five and six orders of magnitude lower than SR-NCF and PBGF-a, respectively. In addition, it is worth noting that the spectrum of HC-HBCF is flatter than PBGF-a and provides a CL < 0.01 dB/km over more than 300 nm (from 1450 nm to 1750 nm), indicating that the presence of anti-resonant cladding suppresses the coupling between core mode and surface mode. The fundamental mode (FM) field profiles of three fibers are shown in right-side panel in Fig. 6. It is noticed that the mode field distribution of HC-HBCF is determined by inner anti-resonant tubes, avoiding the field distortion caused by innermost air hole in bandgap cladding, which usually affects the quality of mode spot in practical applications of HC-PBGF.

The normalized intensity of three fibers with respect to position is depicted in Fig. 7. It is noticed in Fig. 7(a) that the normalized intensity changes from 1 in center of the core to 5.1×10^{-4} in the outermost cladding (y = 37.5 μm) in SR-NCF and changes from 1 to 2.7×10^{-5} in PBGF-a. Moreover, the normalized intensity of HC-HBCF changes in two stages, firstly decreasing from 1 (y = 0 μm) to 2.4×10^{-4} (y = 37.5 μm), and further decreasing to 7.6×10^{-8}. The variation of normalized intensities along x axes presents a same trend as along y axes. Obviously, the hybrid cladding structure effectively achieve combination of two guidance mechanisms: the light is initially confined by the anti-resonant structure of the inner cladding and then further confined by the photonic bandgap structure of the outer cladding, achieving extremely low confinement loss.

Simulating and studying the scattering loss of HC-HBCF is necessary, as its outer cladding is photonic bandgap cladding, the main loss in which is SL caused by surface roughness due

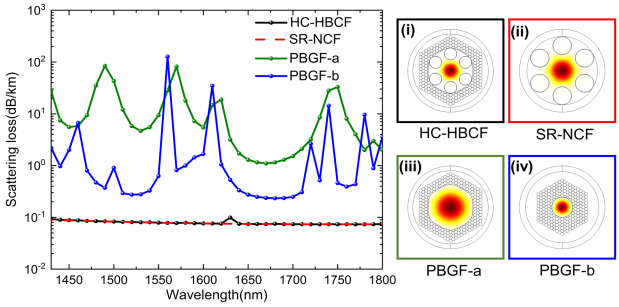

Fig. 8. Comparison of the scattering loss between HC-HBCF, SR-NCF, PBGF-a and PBGF-b. The right-hand side pane illustrates the mode filed profiles of four fibers.

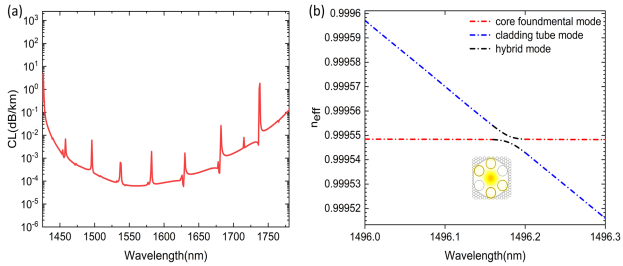

Fig. 9. (a) Simulated confinement loss of HC-HBCF when wavelength scanning interval set as 0.1 nm. (b) Dispersion curves of core fundamental mode and cladding tube mode near 1496.2 nm peak in Fig. 8(a).

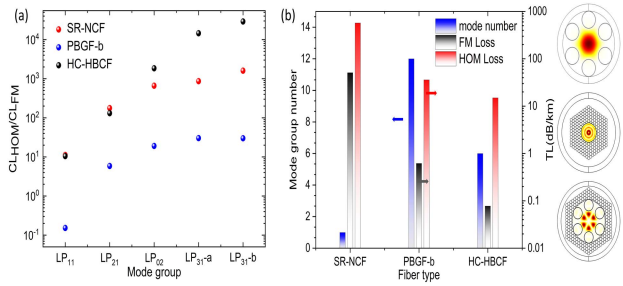

Fig. 10. Comparison of modal content between HC-HBCF, SR-NCF, PBGF-b which have the same core radius of 17.5 μm. (a) The CL ratio between first five high-order mode groups and fundamental mode at 1550 nm of the three fibers. (b) The number of mode group, FM total loss and highest order mode total loss supported by 3 fibers at 1550 nm. The highest order mode field profiles of three fibers are shown in the right panel.

to frozen in capillary waves. The SL spectra of four fibers are shown in Fig. 8. It is noticed that the PBGF-b, with anti-resonant wall thickness, represents less SL, even if the core radius is smaller than PBGF-a. However, due to the presence of more surface modes, its available bandwidth is greatly compressed. While for PBGF-a, despite the number of surface modes is small, the reduction in scattering loss due to a larger core radius is limited, and more guiding modes are introduced at the same time. Moreover, the SR-NCF shows a lower SL than two HC-PBGFs above due to its negative curvature structure and anti-resonant characteristics which effectively reduce the overlap of FM with glass-air surface, and it also maintains flat curve over broad bandwidth that can be seen from Fig. 8.

On the other hand, the proposed HC-HBCF has a same level of scattering loss as SR-NCF. As the inner cladding of proposed HC-HBCF is anti-resonant circular tubes, its anti-resonant effect and negative curvature structure both reduce the light intensity of the air-glass interface. Meanwhile, the HC-HBCF has a large core diameter, which further reduces the mode field intensity at the core-cladding interface. The reduction in the intensity of air-glass interface implies a reduction of F in (4), resulting in a scattering loss of less than 0.1 dB/km for the HC-HBCF. Besides, the coupling between surface mode and guiding mode originally appeared in PBFG-a no longer occurs, and the spectrum is flatter, suggesting that adding an anti-resonant structure inside bandgap cladding can effectively suppress the coupling between core mode and surface mode under special design, thereby greatly increasing the available bandwidth. Therefore, the HC-HBCF has an extremely low total loss (0.1 dB/km) and a wide bandwidth which covers almost the entire bandgap range from 1420 nm to 1800 nm.

During the calculation, we found that the loss spectrum of proposed HC-HBCF is weakly oscillated at some wavelengths. In order to study the oscillation, we set scanning interval from 10 nm to 0.1 nm, and found these oscillations correspond to the anti-crossing coupling between core modes and silica ring-core modes of inner cladding as shown in Fig. 9. However, the bandwidth occupied by anti-cross coupling is extremely narrow due to a more inclined dispersion curve of the cladding silica mode compared to the core fundamental mode and each anti-crossing coupling peak occupies only a few tenths of a nm.Therefore, the influence of these peaks on entire bandwidth can be negligible.

B. Mode Characteristics

In HC-PBGF, the core radius is typically enlarged to reduce scattering loss, which means more core modes are well confined, as the number of air guided modes supported by a HC-PBGF is determined by core dimension, according to the following equation [17]:

$$N_{\max} = \frac{1}{2}\left(\frac{\omega_0 \Lambda}{c}\right)^2 \left(1 - \frac{k_L^2(\omega_0)}{\omega_0^2/c^2}\right)\left(\frac{R_c}{\Lambda}\right)^2 \quad (5)$$

An ideal 37-cell HC-PBGF could theoretically support as many as 80 modes, and the refractive index between high-order modes is so close that they are more susceptible to perturbation-induced coupling. Thus, achieving low loss while controlling the number of modes in HC-PBGF has been extensively studied. Conversely, HC-ANF can only support fundamental mode or a few higher-order modes except for some specific designs as the ability of cladding to confine different modes varies greatly. Therefore, studying the modal properties of hybrid fiber combining two different claddings that have obviously different effects on higher-order modes is significant.

Fig. 10(a) shows confinement loss ratio between the first five high-order mode groups and fundamental mode at 1550 nm for the three fibers. We choose PBGF-b as a comparison fiber because it has a same core radius as the HC-HBCF and the CL of its FM is at a same order of magnitude as that of the HC-HBCF, which is approximately 10^{-5} dB/km. From Fig. 10, we can see that for PBGF-b, the CL_{HOM}/CL_{FM} of first five

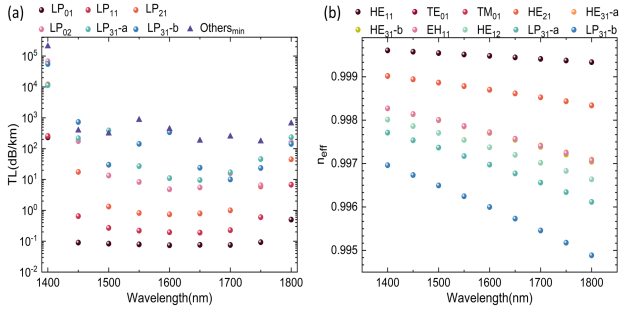

Fig. 11. Modal content of proposed HC-HBCF with three layers of air holes in outer cladding. (a) The total loss of different mode groups with respect to the wavelength. (b) Dispersion curve of different modes.

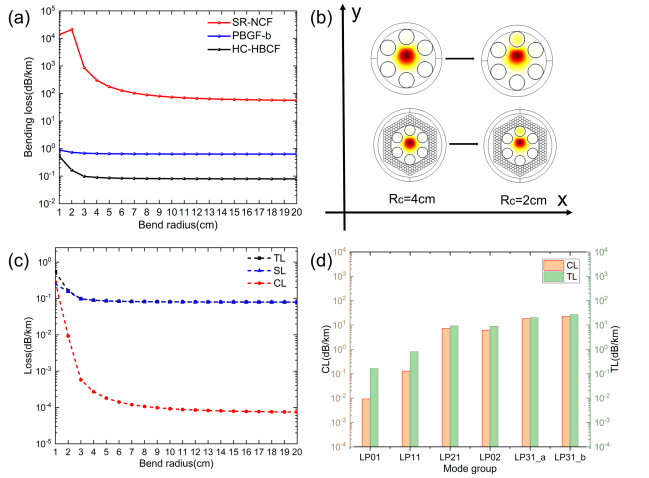

Fig. 12. (a) Bending loss performance of three fibers regarding bend radius. (b) The variation of mode fields of HC-HBCF and SR-NCF as bend radius is changed from 4 cm to 2 cm. (c) TL, SL, CL of HC-HBCF with respect to bend radius at 1550 nm. (d) CL and TL of different modes for HC-HBCF while R_c = 2 cm, wavelength = 1550 nm.

high-order modes are 0.2, 5.9, 19.0, 30.2, 30.0, respectively. Noticeably, due to the unique loss characteristics of TE_{01} mode, its loss is lower than that of the fundamental mode. For SR-NCF, the CL_{HOM}/CL_{FM} of first five high-order modes are 10, 177, 662, 866, 1602, respectively, which is a significant improvement compared to the PBGF-b.

Surprisingly, the result shows that the CL_{HOM}/CL_{FM} of HC-HBCF are 11, 131, 1849, 14556, 29112, respectively, which exhibits a same order of magnitude as that of SR-NCF and even one order of magnitude higher than the SR-NCF for the last two mode group (LP_{31}_a, LP_{31}_b). It indicates that the HC-HBCF has unique advantages and potential for mode control. Due to the great difference in confinement ability of anti-resonant cladding for fundamental mode and high-order modes, the CL of fundamental mode is significantly reduced, while the reduction of high-order mode is less which enlarges the CL ratio between fundamental mode and high-order modes, thereby, the number of low-loss modes can be effectively controlled.

Fig. 10(b) compares the number of mode group, FM total loss and highest order mode total loss supported by three fibers at 1550 nm. Here, high-order modes are considered co-propagating with the fundamental mode if the total loss of the high-order mode is no more than two orders of magnitude higher than fundamental mode. It is noted that PBGF-b can support 12 mode groups. The fundamental mode loss is 0.6 dB/km, and the highest order mode is TE_{03} with a total loss of 20 dB/km. However, the SR-NCF only supports FM, and the loss is 51 dB/km as depicted in Fig. 10(b). The proposed HC-HBCF can support six mode groups half less than PBGF-b. The fundamental mode loss is 0.08 dB/km, and the highest-order mode is LP_{31}-b with a total loss of 18 dB/km. Therefore, the HC-HBCF improves the property of modal content compared with the PBGF-b, and has fewer high-order modes while obtaining a low-loss fundamental mode.

We reduce the outer cladding to three layers to further increase the loss of high-order modes. Fig. 11 shows the mode characteristic of HC-HBCF, which indicates that the proposed fiber can support few-mode transmission. It is noticed that the total loss of LP_{01}, LP_{11}, LP_{21}, LP_{02} are lower than 0.1 dB/km, 1 dB/km, 3 dB/km, 10 dB/km from 1500 nm to 1700 nm respectively. Moreover, the four degenerate LP_{31} modes split into LP_{31}-a and LP_{31}-b, which contain two degenerate modes respectively. It is because the proposed fiber has a c-6v refractive index modulation, makings degeneracy of the LP_{31} which also has a c-6v mode field distribution mode broken. The loss of LP_{31}-a and LP_{31}-b are below 100 dB/km and other high order modes represent losses above 100 dB/km. Meanwhile, the dispersion curves for different modes are shown in Fig. 11(b), from which we can see that the effective refractive index difference between different mode groups is much greater than 10^{-4} order, avoiding crosstalk between different mode groups. Therefore, the HC-HBCF has more design freedom in terms of mode characteristics. We can control the modal content by reasonably designing anti-resonant structure and number of layers of the external bandgap cladding to achieve robust few-mode transmission. The specific design needs further exploration and research.

C. Bending Characteristics

Bending property is a significant factor determining the application of hollow core fibers. Thus, we studied the bending loss for proposed HC-HBCF with comparison to SR-NCF and PBGF-b. To simulate the bending loss, we use a conformal transformation to approximate the refractive index of a bent fiber to that of a straight fiber as described by (6) [26], in which we ignore the electro-optic effect as most of the light are confined in the air core for the hollow core fiber.

$$\mathrm{n}' = n \cdot \mathrm{e}^{\frac{y}{R_c}} \approx n \cdot \left(1 + \frac{y}{R_c}\right) \tag{6}$$

Where n' is conformed refractive index, n is refractive index of the material of straight fiber, R_c represents the curvature radius.

Fig. 12(a) shows the variation of bending loss (BL) with bend radius R_c for three fibers at 1550 nm. It is noticed that the BL for SR-NCF increases continuously as the R_c decreases. When bend radius is 7 cm, the BL increases to 90 dB/km, which is twice as high as $R_c = 20$ cm. Meanwhile, a loss peak can be observed

at 2 cm bend radius due to the coupling between core mode and cladding air mode. However, PBGF-b is almost insensitive to bending as shown in Fig. 12(a). Interestingly, the proposed HC-HBCF exhibits similar bending characteristics with PBGF-b since its loss is almost constant as bend radius decreases, and it still has a very small loss 0.16 dB/km even when the bend radius is 2 cm. Moreover, it also suffers from anti-cross coupling at 1 cm bend radius due to the presence of internal anti-resonant tube. Fig. 12(b) shows the mode fields of HC-HBCF and SR-NCF at $R_c = 4$ cm and $R_c = 2$ cm respectively. We can see that due to anti-crossing effect, the energy of core mode partly leaks into the air mode of anti-resonant tube, resulting in the appearance of peaks in loss spectrum. However, the bending loss remains low due to outer photonic bandgap cladding present in HC-HBCF despite of the presence of anti-crossing effect.

To further illustrate the bending properties of proposed HC-HBCF, we calculated the TL, SL, CL of HC-HBCF with respect to bend radius at 1550 nm. The CL increases slowly as the bend radius decrease and the TL of HC-HBCF is mainly limited by SL. When Rc is less than 2 cm, the CL increases rapidly due to anti-crossing coupling and gradually approaches the SL to jointly determine the TL of proposed fiber. However, the proposed HC-HBCF still exhibits outstanding bending property as the CL and TL is 0.009 dB/km and 0.16 dB/km at Rc = 2 cm. Meanwhile, Fig. 12(d) shows CL and TL of different modes for HC-HBCF while Rc = 2 cm, wavelength = 1550 nm. The TL of LP_{01} and LP_{11} is 0.16 db/km and 0.82 db/km, which is mainly determined by SL instead of CL. Conversely, the TL of LP_{21}, LP_{02}, LP_{31}_a, LP_{31}_b is 9.2 dB/km, 8.9 dB/km, 20.1 dB/km, 27.4 dB/km respectively. For these several higher-order modes, CL accounts for most of TL at Rc = 2 cm. Obviously, the high-order modes of proposed HC-HBCF have similar great bending properties as the fundamental mode, which promote its application in mode-division multiplexed transmission.

IV. Conclusion

In summary, we proposed and numerically investigated a novel hybrid cladding hollow-core fiber, which consists of anti-resonant circular tubes of inner cladding and periodically arranged air holes of outer cladding. The combination of antiresonance and photonic bandgap guidance mechanisms is effectively achieved in the proposed fiber by direct physical contact of the two claddings. The simulation results show that the confinement loss of the HC-HBCF is five and six orders of magnitude lower than those of the two fibers with separate cladding respectively. The scattering loss is maintained below 0.1 dB/km from 1430 nm to 1780 nm and the spectrum remains relatively flat. It indicates that the internal anti-resonant structure makes the core mode unaffected by the surface modes of the bandgap cladding, which will ease the fabrication difficulty as the inner air holes of the bandgap cladding easily deformed when the core size becomes larger. The HC-HBCF exhibits excellent bending characteristics with a loss of 0.16 dB/km at a bend radius of 2 cm. In addition, the simulation results on modal content show that the HC-HBCF has more design freedom in terms of mode characteristics as we can control the fiber modes by reasonably designing the anti-resonant structure and the number of layers of the external bandgap cladding. We believe the proposed HC-HBCF with ultralow loss, wide bandwidth, low bending loss and outstanding modal content will provide a new direction for the design and fabrication of hollow-core fibers.

References

[1] R. F. Cregan et al., "Single-mode photonic band gap guidance of light in air," *Science*, vol. 285, pp. 1537–1539, 1999.

[2] A. Iyer, W. Xu, J. E. Antonio-Lopez, R. A. Correa, and W. H. Renninger, "Ultra-low Brillouin scattering in anti-resonant hollow-core fibers," *APL Photon.*, vol. 5, 2020, Art. no. 096109.

[3] B. J. Mangan et al., "First demonstration of hollow-core fiber for intra data center low latency connectivity with a commercial 100 Gb/s interface," in *Proc. Opt. Fiber Commun. Conf. Exhib.*, 2015, pp. 1–3.

[4] E. Numkam Fokoua, V. Michaud-Belleau, J. Genest, R. Slavík, and F. Poletti, "Theoretical analysis of backscattering in hollow-core antiresonant fibers," *APL Photon.*, vol. 6, 2021, Art. no. 096106.

[5] F. Poletti et al., "Towards high-capacity fibre-optic communications at the speed of light in vacuum," *Nature Photon.*, vol. 7, pp. 279–284, 2013.

[6] D. Wu, F. Yu, and M. Liao, "Understanding the material loss of anti-resonant hollow-core fibers," *Opt. Exp.*, vol. 28, pp. 11840–11851, 2020.

[7] Y. Chen et al., "Multi-kilometer long, longitudinally uniform hollow core photonic bandgap fibers for broadband low latency data transmission," *J. Lightw. Technol.*, vol. 34, no. 1, pp. 104–113, Jan. 2016.

[8] Z. Liu et al., "Nonlinearity-free coherent transmission in hollow-core antiresonant fiber," *J. Lightw. Technol.*, vol. 37, no. 3, pp. 909–916, Feb. 2019.

[9] H. C. H. Mulvad et al., "Kilowatt-average-power single-mode laser light transmission over kilometre-scale hollow-core fibre," *Nature Photon.*, vol. 16, pp. 448–453, 2022.

[10] F. Gebert et al., "Damage-free single-mode transmission of deep-UV light in hollow-core PCF," *Opt. Exp.*, vol. 22, pp. 15388–15396, 2014.

[11] B. Kuiri et al., "Development of ring-core photonic crystal fiber based on LiNbO3 supporting higher-order OAM modes," *Opt. Quantum Electron.*, vol. 55, 2023, Art. no. 726.

[12] P. S. J. Russell, P. Hölzer, W. Chang, A. Abdolvand, and J. C. Travers, "Hollow-core photonic crystal fibres for gas-based nonlinear optics," *Nature Photon.*, vol. 8, pp. 278–286, 2014.

[13] F. Yang, F. Gyger, and L. Thevenaz, "Intense Brillouin amplification in gas using hollow-core waveguides," *Nature Photon.*, vol. 14, pp. 700–708, 2020.

[14] Y. Zhao, Y. Qi, H. L. Ho, S. Gao, Y. Wang, and W. Jin, "Photoacoustic Brillouin spectroscopy of gas-filled anti-resonant hollow-core optical fibers," *Optica*, vol. 8, pp. 532–538, 2021.

[15] F. Poletti, M. N. Petrovich, and D. J. Richardson, "Hollow-core photonic bandgap fibers: Technology and applications," *Nanophotonics*, vol. 2, pp. 315–340, 2013.

[16] P. Roberts et al., "Ultimate low loss of hollow-core photonic crystal fibres," *Opt. Exp.*, vol. 13, pp. 236–244, 2005.

[17] M. N. Petrovich, F. Poletti, A. van Brakel, and D. J. Richardson, "Robustly single mode hollow core photonic bandgap fiber," *Opt. Exp.*, vol. 16, pp. 4337–4346, 2008.

[18] J. West, C. Smith, N. Borrelli, D. Allan, and K. Koch, "Surface modes in air-core photonic band-gap fibers," *Opt. Exp.*, vol. 12, pp. 1485–1496, 2004.

[19] B. J. Mangan et al., "Low loss (1.7 dB/km) hollow core photonic bandgap fiber," in *Proc. Opt. Fiber Commun. Conf.*, 2004, Paper PD24.

[20] B. Debord et al., "Ultralow transmission loss in inhibited-coupling guiding hollow fibers," *Optica*, vol. 4, pp. 209–217, 2017.

[21] N. M. Litchinitser, A. K. Abeeluck, C. Headley, and B. J. Eggleton, "Antiresonant reflecting photonic crystal optical waveguides," *Opt. Lett.*, vol. 27, pp. 1592–1594, 2002.

[22] F. Benabid, J. C. Knight, G. Antonopoulos, and P. S. Russell, "Stimulated Raman scattering in hydrogen-filled hollow-core photonic crystal fiber," *Science*, vol. 298, pp. 399–402, 2002.

[23] S. Fevrier, B. Beaudou, and P. Viale, "Understanding origin of loss in large pitch hollow-core photonic crystal fibers and their design simplification," *Opt. Exp.*, vol. 18, pp. 5142–5150, 2010.

[24] Y. Y. Wang, N. V. Wheeler, F. Couny, P. J. Roberts, and F. Benabid, "Low loss broadband transmission in hypocycloid-core Kagome hollow-core photonic crystal fiber," *Opt. Lett.*, vol. 36, pp. 669–671, 2011.

[25] A. D. Pryamikov, A. S. Biriukov, A. F. Kosolapov, V. G. Plotnichenko, S. L. Semjonov, and E. M. Dianov, "Demonstration of a waveguide regime for a silica hollow–core microstructured optical fiber with a negative curvature of the core boundary in the spectral region >3.5 μm," *Opt. Exp.*, vol. 19, pp. 1441–1448, 2011.

[26] F. Poletti, "Nested antiresonant nodeless hollow core fiber," *Opt Exp.*, vol. 22, pp. 23807–23828, 2014.

[27] S. F. Gao et al., "Hollow-core conjoined-tube negative-curvature fibre with ultralow loss," *Nature Commun.*, vol. 9, 2018, Art. no. 2828.

[28] G. T. Jasion et al., "Hollow core NANF with 0.28 dB/km attenuation in the C and L bands," in *Proc. Opt. Fiber Commun. Conf. Expo.*, 2020, pp. 1–3.

[29] H. Sakr et al., "Hollow core NANFs with five nested tubes and record low loss at 850, 1060, 1300 and 1625 nm," in *Proc. Opt. Fiber Commun. Conf. Exhib.*, 2021, pp. 1–3.

[30] K. S. R. Shaha, A. Khaleque, and M. S. Hosen, "Wideband low loss hollow core fiber with nested hybrid cladding elements," *J. Lightw. Technol.*, vol. 39, no. 20, pp. 6585–6591, Oct. 2021.

[31] W. Zheng et al., "Wideband low confinement loss anti-resonant hollow core fiber with nested U-shape tube," *Opt. Exp.*, vol. 29, pp. 24182–24192, 2021.

[32] Y. Zhu, N. Song, F. Gao, and X. Xu, "Low loss hollow-core antiresonant fiber with nested supporting rings," *Opt. Exp.*, vol. 29, pp. 1659–1665, 2021.

[33] F. Amrani et al., "Low-loss single-mode hybrid-lattice hollow-core photonic-crystal fibre," *Light: Sci. Appl.*, vol. 10, 2021, Art. no. 7.

[34] J. G. Hayashi, S. M. A. Mousavi, A. Ventura, and F. Poletti, "Numerical modeling of a hybrid hollow-core fiber for enhanced mid-infrared guidance," *Opt. Exp.*, vol. 29, pp. 17042–17052, 2021.

[35] T. P. White et al., "Multipole method for microstructured optical fibers. I. Formulation," *Opt. Lett.*, vol. 19, pp. 2322–2320, 2002.

[36] J. R. Hayes et al., "Antiresonant hollow core fiber with an octave spanning bandwidth for short haul data communications," *J. Lightw. Technol.*, vol. 35, no. 3, pp. 437–442, Feb. 2017.

[37] M. H. Frosz et al., "Five-ring hollow-core photonic crystal fiber with 1.8 dB/km loss," *Opt. Lett.*, vol. 38, pp. 2215–2217, 2013.